ELSEVIER

Earth and Planetary Science Letters 210 (2003) 167–178

EPSL

www.elsevier.com/locate/epsl

Zinc isotope variations in deep-sea carbonates from the eastern equatorial Pacific over the last 175 ka

Sylvain Pichat [a,b,*], Chantal Douchet [a], Francis Albarède [a]

[a] *Laboratoire de Sciences de la Terre, Ecole normale supérieure de Lyon, 46 allée d'Italie, 69364 Lyon Cedex 07, France*
[b] *Max Planck Institut für Chemie, Abteilung Geochemie, Postfach 3060, D-55020 Mainz, Germany*

Received 26 September 2002; received in revised form 19 February 2003; accepted 3 March 2003

Abstract

The carbonate fraction of sediment core ODP 849, leg 138, located in the eastern equatorial Pacific, mostly consisting of coccoliths, was separated and analyzed for its Zn isotopic composition. The overall variation in Zn isotopic composition, as determined by multiple-collector, magnetic-sector, inductively coupled plasma mass spectrometry, was found to be on the order of 1‰ (expressed in δ^{66}Zn, where $\delta^{x}Zn = [(^{x}Zn/^{64}Zn)_{sample}/(^{x}Zn/^{64}Zn)_{standard} - 1] \times 10^{3}$ and $x = 66$, 67 or 68) over the last 175 ka. The analytical precision was 0.04‰ and the overall reproducibility was usually better than 0.07‰. The Zn isotopic composition signal exhibits several marked peaks and a high-frequency variability. A periodogram of the δ^{66}Zn signal showed two periodicities of 35.2 and 21.2 ka. We suggest that the latter is caused by the precession of the Earth's axis of rotation. The periodogram exhibits a minimum at 41.1 ka, thus showing that the Zn isotopic composition is independent of the obliquity in the eastern equatorial Pacific. The range of δ^{66}Zn values observed for the carbonate fraction of ODP 849 overlaps with the range observed for Fe–Mn nodules in the world's oceans, which suggests that seawater/carbonate Zn isotope fractionation is weak. We therefore assume that most of the Zn isotope variability is a result of the selective entrainment of the light isotopes by organic matter in the surface ocean. The ODP 849 δ^{66}Zn record seems to follow the changes in the insolation cycles. Changes in the late summer/fall equatorial insolation modulate the intensity of the equatorial upwelling, hence the mixing between deep and surface waters. We propose that during decreased summer/fall equatorial insolation, when a steep thermocline can develop (El Niño-like conditions), the surface waters cannot be replenished by deep waters and become depleted in the lighter Zn isotopes by biological activity, thus resulting in the progressive increase of the δ^{66}Zn values of the carbonate shells presumably in equilibrium with surface seawater.

Keywords: Zn isotopes; carbonates; thermocline; precession; insolation; ENSO

1. Introduction

The equatorial Pacific is nowadays the main area where CO_2 is transferred to the atmosphere [1]. The exchanges of CO_2 between the ocean and the atmosphere are influenced by the biological productivity which in turn is affected by climate

* Corresponding author. Tel.: +49-6131-305-204; Fax: +49-6131-371-051.
E-mail address: spichat@mpch-mainz.mpg.de (S. Pichat).

0012-821X/03/$ – see front matter © 2003 Elsevier Science B.V. All rights reserved.
doi:10.1016/S0012-821X(03)00106-7

changes. The study of the biogeochemical cycle of elements that are involved in marine biological processes appears therefore fundamental to better understand the variations of the climate.

Fe is thought to limit biological productivity in high-nutrient–low-chlorophyll areas [2] like the Southern Ocean or the eastern equatorial Pacific. A similar limitation of the biological productivity by Zn, called the 'zinc hypothesis', has been proposed by Morel et al. [3]. Zn is depleted from surface waters by the biological pump and is regenerated in the deep ocean through oxidation of organic matter by bacterial activity and the dissolution of sinking particles [4]. Zn also mimics Si, a non-labile macronutrient, as shown by the similarity between water column profiles of these elements [4]. It has also been demonstrated that Zn participates in multiple biological processes [5], notably as cofactor in enzymatic photosynthetic reactions. In particular, Zn is a cofactor in the carbonic anhydrase [6] that catalyzes the conversion between HCO_3^- and CO_2. For instance, in coccolithophoridae, carbonic anhydrase facilitates the use of HCO_3^- in photosynthesis [7]. It has been argued that fractionation between light and heavy isotopes of Zn in particles collected in sediment traps is stronger after biological blooms with a time lag of a few weeks likely corresponding to the time required for the homogenization of the Zn concentration [8]. This feature has been interpreted as reflecting the rapid depletion of surface waters in the lightest Zn isotope during biological blooms because of its preferential uptake in biochemical reactions. The variations in the biological fractionation could be recorded in deep-sea sediments, therefore allowing us to monitor change in biological productivity.

The approach chosen in this study was to analyze the Zn isotopic composition of the carbonate fraction of the sediment. Since the carbonate fraction is mostly composed of shells and fragments of shells, it is the most likely to have recorded biologically linked changes in the Zn isotopic composition. Our study was focused on the eastern equatorial Pacific, a high-nutrient–low-chlorophyll area where the productivity is thought to be limited by micronutrient [9]. The motivation of our work was to determine whether downcore, i.e. temporal, Zn isotopic variations exist in the carbonate fraction of the sediment and, if so, whether this variability could be used as a paleoceanographic proxy. Zn is ubiquitous; therefore, the first stage of this work was to separate the carbonate fraction of the sediment while avoiding Zn contamination from other fractions and from chemical reactants. We used multiple-collector inductively coupled plasma mass spectrometry (MC-ICP-MS), which achieves the high precision required to measure Zn isotopic variations [10]. After having established the amplitude and the timing of these variations, we suggest a mechanism that drives the variability and establish the relationships with the biological activity. Potential links with the climate variability during the Quaternary are discussed.

2. Experimental

2.1. Samples

Cores from ODP leg 138 site 849, holes B and C, hereafter referred to as ODP 849, have been used for this study because of their high carbonate content (65–85%) [11,12]. ODP 849 is located in the eastern equatorial Pacific, under the equatorial undercurrent and the equatorial upwelling (Fig. 1). This site has been lying above the carbonate compensation depth throughout its history [11]. It also offers the advantage of being located far from riverine sources that could have imported Zn with a terrigenous isotopic signature, and 860 km west of the East Pacific Rise, i.e. far from hydrothermal sources that could have been a source of mantle-derived Zn.

2.2. Age model and stratigraphy

The sections analyzed for Zn isotope composition are the first two sections (4–142 cm and 1–134 cm) of ODP 849 hole B, and sections 2 and 3 of hole C (14–143 cm and 11–122 cm). In spite of local variations in the lithology and the biostratigraphy [11], the sections remain dominated by coccoliths and foraminifer fragments. The age model has been established on the analyzed sec-

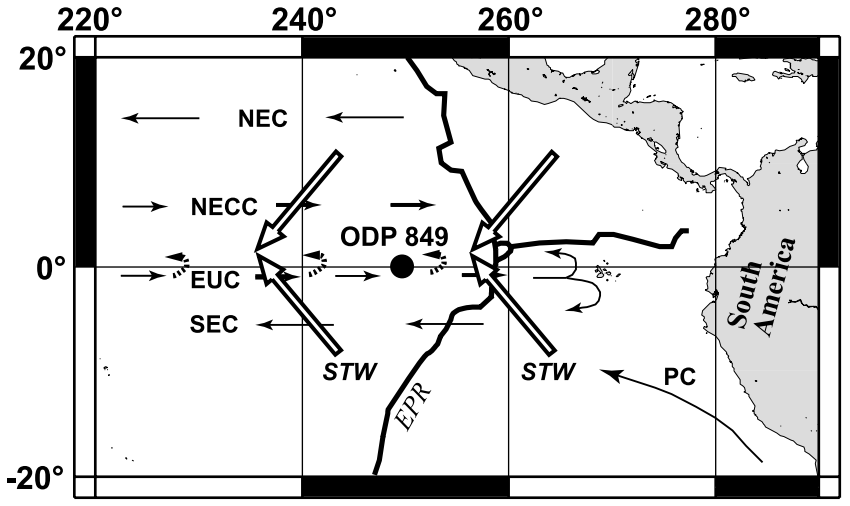

Fig. 1. The eastern equatorial Pacific. The solid circle shows the location of the ODP 849 site (0°11.59′N, 110°31.18′W, 3851 m water depth). The solid arrows represent the paths of the main surface currents: the north equatorial current (NEC), the north equatorial countercurrent (NECC), the equatorial undercurrent (EUC), the south equatorial current (SEC) and the Peru current (PC). The dashed arrows represent the equatorial upwelling, which originates from the EUC [13]. The open arrows show the direction of the trade winds (STW: southeast trade winds). The solid line represents the East Pacific Rise (EPR).

tions by oxygen isotope stratigraphy on benthic foraminifera *Cibicides wuellestorfi* [14]. Correlations between the cores recovered from the two holes were made by using the revised metric composite depth scale [15].

3. Analytical

Zn has five stable isotopes of mass 64 (48.63%), 66 (27.90%), 67 (4.10%), 68 (18.75%) and 70 (0.62%) [16]. For this study, we use the $^{66}Zn/^{64}Zn$ ratio to compare samples, but we also checked the $^{67}Zn/^{64}Zn$ and the $^{68}Zn/^{64}Zn$ ratios to assess the reliability of our data (Section 3.3).

3.1. Carbonate fraction vs. single shell/organism analysis

MC-ICP-MS appears now as the most accurate means of determining the Zn isotopic composition of geological materials [10]. However, because of the low natural abundance of ^{67}Zn the amount of Zn required is at least 100 ng on the Plasma 54 (VG Elemental) in order to perform a reproducible, precise analysis, i.e. with good counting statistics, and to avoid blank correction problems. Based on literature data for the Zn/Ca ratio (average: 4.4 μmol/mol) [17,18] the Zn content of a single shell of a foraminifer is estimated to be on the order of 0.14 ng (assuming a shell weight of 50 μg with 95% $CaCO_3$), i.e. still too low to be measured on the current generation of MC-ICP-MS.

Because Zn isotopic composition, so far, cannot be measured on amounts of Zn corresponding to a single shell and because reconnaissance investigations are needed for elements with unknown isotope geochemistry, we trusted that the downcore Zn isotope variations on the bulk carbonate fraction of the sediment was an important first step.

3.2. Carbonate fraction dissolution and Zn separation

The sediment samples were first dried in an oven at 60–70°C for 3 days. They were then crushed in an agate mortar which has been previously cleaned with successive treatments of acid washed silica, ethanol, and Milli-Q water, and then pre-contaminated with a small portion of

the sample, in order to avoid sample cross-contamination. The resulting powder was then thoroughly homogenized.

We first tested on bulk sediment the procedure originally proposed by Boyle and Keigwin [19] to clean foraminifers and dissolve their carbonate fraction. However, the reproducibility of the analyses performed using this technique turned out to be inadequate (Fig. 2). We therefore developed a new selective dissolution procedure for the carbonate fraction of the sediment. 150–400 mg of the sediment powder was agitated and ultrasonicated in 3–5 ml of Milli-Q water (18.2 MΩ cm) for 5 min and the supernatant was removed after 5 min of centrifugation. This operation was repeated twice with Milli-Q water and once with ethanol in between. These steps eliminate hydrosoluble salts and fine grains of clay. Carbonates were then selectively dissolved by 6–8 h leaching in 2–3 ml of 1–2 M acetic acid in a closed Teflon PFA beaker at 60–70°C. The supernatant was kept for Zn isotopic analysis. The total dissolution of the carbonate in the residual solid was ensured by adding 1–2 M of acetic acid (1–3 ml) until no CO_2 bubbles evolved after mechanical shaking. The sample was then maintained for ca. 4 h on a hotplate at 60–70°C. We have used dilute acetic acid at low temperature in order to avoid attacking (1) the lattice structures of the clay minerals [20] and (2) the ferromanganese coatings or micronodules [21]. The supernatant fractions collected from the two acetic acid leaches were combined, evaporated to dryness at 60–70°C and then dissolved in 4–5 ml of 7 M HCl–0.01‰ H_2O_2. Hydrogen peroxide was used to eliminate the potential remaining organic matter. The evaporation–dissolution process was repeated twice to achieve the conversion to chloride form. Finally, the sample was recovered in 1–2 ml of 7 M HCl–0.01‰ H_2O_2 before the separation of Zn by anion-exchange chromatography, as described by Maréchal et al. [10].

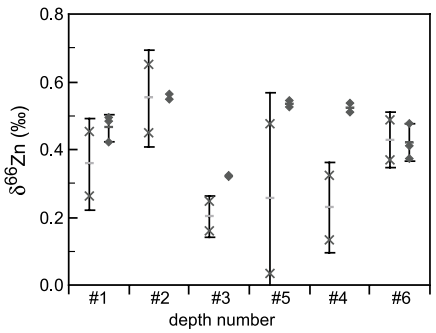

Fig. 2. Comparison of the reproducibility of two procedures of dissolution of the carbonate fraction of deep-sea sediment. Samples taken at six different depths (#1 to #6) in core MD972138 (1°25′S, 146°24′E, 1900 m water depth) were used for the comparison. Each cross or lozenge represents one full replicate analysis (dissolution, chromatographic separation and spectrometry). The average $\delta^{66}Zn$ values are represented by a dash and the error bars represent the standard deviations. For each depth, the data obtained with the procedure of Boyle and Keigwin [19] are on the left (crosses) and the data obtained with the procedure used in this study are on the right (lozenges). For each depth, two full replicates were analyzed for each procedure except for sample #6, where three full replicates were analyzed for the procedure used in this study.

This method was found to have a better reproducibility than the method of Boyle and Keigwin [19] (Fig. 2). The procedure was developed by these authors to clean hand-picked foraminifera shells with a total sample weight of 0.2–0.5 mg. We suspect that the same cleaning procedure applied to 150–400 mg of bulk sediment leads to the partial dissolution of particular phases. On average, the $\delta^{66}Zn$ values found using the Boyle and Keigwin [19] method were lower than the values found using our method and sometimes fall within the values of the terrigenous material (0.24 ± 0.06‰) that has been compiled after the data of Maréchal et al. [8]. High and variable levels of contamination due to the variety and the large amounts of reagents (solution of citric acid–ammonium hydroxide–hydrazine) used in the Boyle and Keigwin [19] method can also have contributed to the lack of reproducibility. Sample heterogeneity is unlikely to be critical since it should affect the results regardless of the method. We can rule out a massive contamination as the source of the good reproducibility in our dissolution method: (1) The $\delta^{66}Zn$ values of the carbonate fraction fall far of the field of the terrigenous material, thus showing that the latter is not contaminating the carbonate fraction. (2) Leaching ferromanganese crusts with 1 M acetic acid releases no visible Mn and only traces of Fe on a few samples [22], which shows that Fe–Mn

crusts are left essentially untouched by our dissolution process. (3) Even in the case of a partial dissolution of the Fe–Mn coatings or micronodules, a simple mass-balance calculation rules out a massive contamination by Zn linked to these coatings or micronodules. Our samples (average 300 mg) contain less than 0.5 wt% Fe and Mn (average 0.25 wt%) [12]. Assuming that the Fe–Mn coatings with an average of 750 ppm Zn [8] are dissolved at 10%, they contribute less than 5–10% to our samples (ca. 0.5–1 μg Zn). Since the ranges of Zn isotope compositions in nodules and carbonates are similar, the effect on the present isotopic result should be small.

The samples were processed in a clean room under laminar flow hood to minimize Zn contamination. Special care was taken to avoid contact between the samples and gloves [23] or Parafilm®. Teflon FEP bottles used to store the acids, centrifuge tubes and pipet tips were cleaned twice with double-distilled 6 M HCl prior to their use. Teflon PFA beakers were cleaned in successive baths of double-distilled HNO_3 and HCl. The acids were double-distilled in Vycor stills except the reagent-grade acetic acid, which was purified for Zn by eluting 0.5 l through two successive AG1×8 (100–200 mesh, chloride form) columns of 2 ml. The concentration of Zn in the acetic acid is reduced to 0.1 ng/g by this means, i.e. 20–15 times less than the unpurified acetic acid. Acids and overall procedural blanks have been repeatedly measured by quadrapole ICP-MS (Plasma Quad, VG Elemental). Acid purity was checked after the preparation of each new batch. For each session of sample preparation, corresponding to 10–15 samples, two to three overall procedural blanks were measured. The overall procedural blanks were systematically less than 15 ng for Zn, and therefore contributed less than 3% of the total Zn analyzed.

3.3. Mass spectrometry

Zn isotopic compositions were determined by MC-ICP-MS (Plasma 54) using the analysis protocol described by Maréchal et al. [10]. The samples were dissolved in 0.05 N HNO_3 and were injected by free aspiration in a glass expansion nebulizer. The ^{64}Zn signal was corrected for a ^{64}Ni contribution [10], but this contribution was negligible. We used the method described by Maréchal et al. [10] to correct for instrumental mass fractionation. This method is now used for various isotopic systems to look at small isotopic fractionation, e.g. [24]. The purified Zn samples were doped with a Cu standard solution (NIST no. 976) and the $^{65}Cu/^{63}Cu$ ratio was used to monitor the instrumentally induced mass fractionation of Cu. Accuracy was further improved by bracketing each sample analysis with the measurement of a reference mixed Zn–Cu standard solution. We found that the fractionation factors for Cu and Zn remain in a constant ratio over 1 day of measurement, but not from one day to another, as already shown by Maréchal et al. [10]. The results are given in the conventional delta notation:

$$\delta^{66}Zn = 10^3 \times \left(\frac{(^{66}Zn/^{64}Zn)_{sample}}{(^{66}Zn/^{64}Zn)_{JMC}} - 1 \right) \quad (1)$$

where JMC designates the Zn JMC 3-0749L standard solution. $\delta^{66}Zn$ was chosen because of the higher natural abundance of ^{66}Zn compared to ^{67}Zn and ^{68}Zn. The latter two isotopes, however, were used to verify the validity of the measurements. In particular, mass-dependent fractionation was checked for all samples against $\delta^{67}Zn$ and $\delta^{68}Zn$. The samples presented in this study lie along a line $\delta^{67}Zn = 1.47 \pm 0.09$ ($R^2 = 0.90$, $N = 77$) × $\delta^{66}Zn$ in the $\delta^{67}Zn$ vs. $\delta^{66}Zn$ space, and $\delta^{68}Zn = 1.92 \pm 0.07$ ($R^2 = 0.96$, $N = 77$) × $\delta^{66}Zn$ in the $\delta^{68}Zn$ vs. $\delta^{66}Zn$ space. Our results nicely fit a mass-dependent fractionation law which predicts that the slopes in such diagrams are proportional to the mass difference, ca. 1.5 and 2.0, respectively.

4. Results

The results are reported in Table 1 and plotted in Fig. 3 as a function of the deposition age. The values of $\delta^{66}Zn$ range from 0.31 to 1.34‰ with several marked peaks. The range of variation is larger by a factor of 25 than the overall analytical precision of 0.04‰. The amplitude of the $\delta^{66}Zn$

Table 1
δ^{66}Zn values (‰) and age (ka) of core ODP 849

Sample name	δ^{66}Zn (‰)	2σ err.	*N*	Age (ka)	Sample name	δ^{66}Zn (‰)	2σ err.	*N*	Age (ka)
ODP 004 F-ave.	0.32	0.07	2	3.0	ODP 292	0.98			85.4
ODP 042 F-ave.	0.66	0.01	2	10.5	ODP 322-HC	1.14			97.1
ODP 052	0.87			12.5	ODP 331-HC	1.05			101.3
ODP 062 F-ave.	0.94	0.07	4	14.6	ODP 342-HC	1.25			106.5
ODP 072	0.91			17.1	ODP 352-HC F-ave.	0.99	0.06	2	111.0
ODP 082	0.83			18.9	ODP 362-HC	1.19			114.9
ODP 102 F-ave.	0.61	0.07	4	23.6	ODP 372-HC	1.19			118.8
ODP 112	0.51			26.0	ODP 382-HC A-ave.	1.06	0.01	2	122.0
ODP 122 F-ave.	0.73	0.08	2	28.6	ODP 392-HC F-ave.	1.03	0.06	2	125.4
ODP 131	0.79			31.3	ODP 402-HC	0.81			127.9
ODP 142 F-ave.	0.35	0.13	2	34.4	ODP 412-HC	1.03			130.0
ODP 152a	0.52			37.7	ODP 422-HC	0.87			132.5
ODP 152	0.71			38.5	ODP 432-HC F-ave.	0.90	0.05	2	134.5
ODP 162 F-ave.	0.98	0.05	8	41.1	ODP 442-HC	0.89			137.0
ODP 170	0.69			44.1	ODP 452-HC	0.85			139.2
ODP 182	0.63			48.6	ODP 472-HC	0.89			144.4
ODP 192 A-ave.	0.83	0.03	2	52.2	ODP 482-HC A-ave.	1.02	0.05	2	147.1
ODP 202	0.70			55.8	ODP 493-HC A-ave.	1.08	0.02	2	150.2
ODP 212 F-ave.	0.97	0.24	2	59.2	ODP 513-HC	1.24			155.8
ODP 222	0.75			63.2	ODP 523-HC	1.09			158.6
ODP 232 F-ave.	0.91	0.11	2	66.4	ODP 533-HC	1.34			161.4
ODP 242 F-ave.	0.54	0.03	2	69.4	ODP 543-HC	1.21			164.2
ODP 245 A-ave.	0.67	0.04	2	70.6	ODP 552-HC A-ave.	1.18	0.01	2	166.5
ODP 252 F-ave.	0.97	0.04	2	72.6	ODP 562-HC A-ave.	1.24	0.04	3	169.0
ODP 255	0.90			73.6	ODP 572-HC A-ave.	1.21	0.06	2	171.3
ODP 272 F-ave.	1.15	0.25	2	78.9	ODP 583-HC A-ave.	1.05	0.08	2	173.8

'F-ave.' stands for average value of full replicate analyses (dissolution, chromatographic separation and spectrometry). 'A-ave.' stands for average value of the replicate analyses. In both cases, the average values are reported together with the 2σ error, denoted 2σ err., and the number of full replicates, denoted *N*. '-HC' indicates that the sample comes from hole C. Other samples come from hole B.

variations over ~10 ka can be as high as 0.6‰. The record shows a general downcore trend of increasing values and decreasing amplitude variations. The older samples show the highest δ^{66}Zn values ever reported for terrestrial material. During the Isotopic Stage 5, the δ^{66}Zn signal appears to be more stable. However, this phenomenon might be an artifact due to the lower sampling density. The average δ^{66}Zn value for the carbonate fraction of core ODP 849 (0.91 ± 0.24‰) markedly departs from the average value of terrigenous materials (0.24 ± 0.06‰). Note that all the values measured in core ODP 849 lie out of the range of those of the terrigenous material. The full replicate analyses (dissolution, chromatographic separation and spectrometry) show that the overall reproducibility was better than 0.07‰ (2σ level) when more than two replicate analyses were performed. The reproducibility is only 75% larger than the analytical precision and therefore indicates that the sample heterogeneity was not very significant. Four samples replicated once (ODP 142, ODP 212, ODP 232, and ODP 272) show more heterogeneity and/or lower reproducibility; however, most of the replicate analyses show reproducibility better than 0.07‰ (2σ level). All the replicate analyses are reported in Table 1.

5. Discussion

Until now, Zn isotopic compositions were only known for two sediment cores, one from the trop-

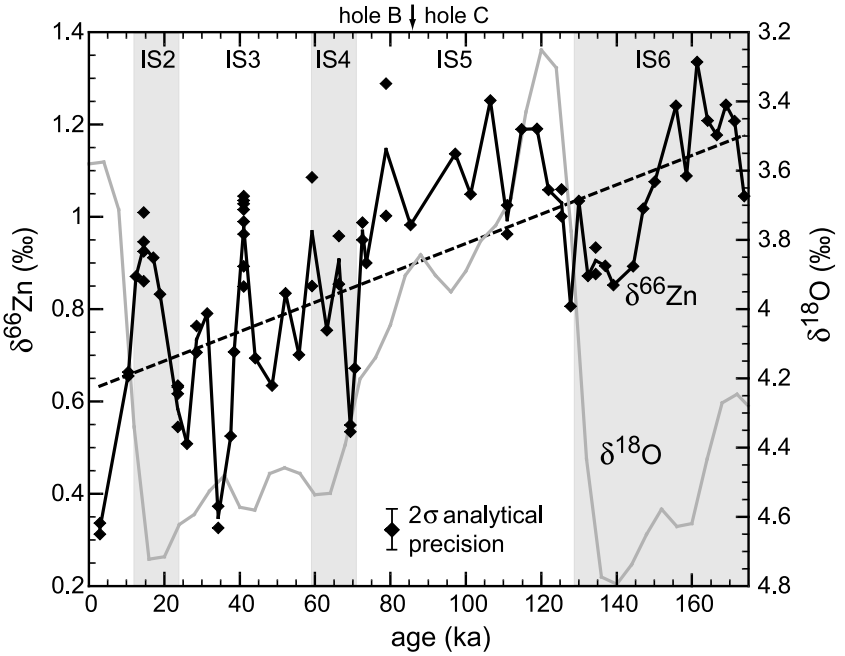

Fig. 3. δ^{66}Zn (solid lozenges) in the carbonate fraction of the ODP 849 core over the last 175 ka. The solid line runs through the average values of the replicates. The dashed line is the linear trend removed to calculate the periodogram: $\delta^{66}Zn = 0.544 \times t + 0.633$, where t is the age normalized to the age window (170.8 ka). The gray curve is the δ^{18}O record [14]. The ages have been interpolated using the revised metric composite depth scale [15]. The even-numbered isotopic stages (IS) are glacial periods and are emphasized with a gray shade. The IS scale is from Imbrie et al. [25]. Note the transition between analyses made on holes B and C sediment samples ($\sim$86 ka). The small variations in the lithology and the biostratigraphy [11] are not reflected in the δ^{66}Zn values. The age correlation between the two holes was established using the revised metric composite depth scale [15].

ical Atlantic and the other from the tropical Pacific [8], in which they show no significant variability with depth/time. These measurements were made on bulk sediment and the mean values of δ^{66}Zn in these two cores, 0.22 ± 0.03‰ for the Atlantic (KTB14) and 0.26 ± 0.07‰ for the Pacific (RC17-203), lie within the range of terrigenous material. Since both cores are dominated by either red clay – Pacific core – or lithogenic material – Atlantic core – it can be concluded that the Zn isotopic compositions measured in both cores are mainly reflecting the composition of the terrigenous fraction of the sediment. Therefore, it appears that the difference between these results and ours shows that the δ^{66}Zn signal of the terrigenous fraction of the sediment obliterates the potential δ^{66}Zn signal linked to biological activity and supports our choice of removing the terrigenous fraction of the sediment to study the biogeochemical cycle of Zn. Maréchal et al. [8] have measured δ^{66}Zn in surface scrapping of Fe–Mn nodules and assumed that the Fe–Mn nodules were equilibrated with seawater. On this basis they inferred that the depletion of the light Zn isotopes in Fe–Mn nodules results from the biological activity in the upper water column. Marchitto et al. [17] have also shown that the Zn/Ca ratio in benthic foraminifers reflects the deep-water (ambient) dissolved Zn levels. Calcareous nannofossils, mostly constituted of coccolithophoridae, deposit calcium carbonate with oxygen and carbon at or near equilibrium with oceanic surface waters [26]. Zn is largely present in seawater as hydroxide and carbonate complexes [27] and these have been shown to have minimal fractionation in aqueous solutions [28,29], which is supported by the similarity between the mean δ^{66}Zn value of our carbonate rec-

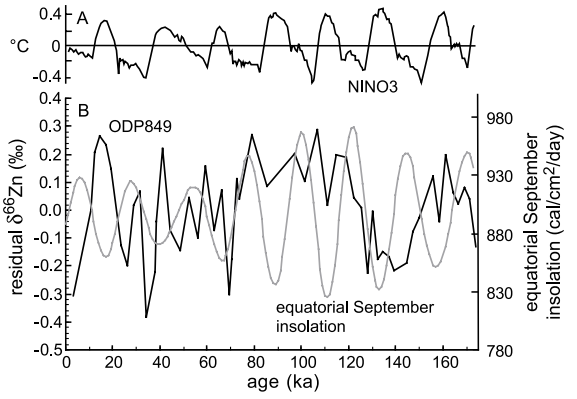

Fig. 4. (A) Residual δ^{66}Zn signal (black line) after removal of the linear secular trend. The average value of the residuals is 2×10^{-5}. The gray line is the equatorial September insolation [41] (upwelling season). (B) 500-yr average NINO3 index forced with Milankovitch solar forcing [38].

ord (0.91‰) and the one of the Fe–Mn nodules in the east tropical Pacific (0.82‰, $n=8$ [8]). We therefore assume that the Zn isotopic composition of the carbonate fraction, which is predominantly constituted of coccoliths and foraminifer fragments, and seawater in which the shell was built are similar. This similarity also tends to suggest that the 'vital effect' during shell growth is likely to be small.

The glacial/interglacial variations of the sea surface temperature (SST) in the eastern equatorial Pacific are 3–5°C [30] or even lower (1.2 ± 0.3°C) [31] for the Last Glacial Maximum (LGM)–Holocene transition. Temperature is known to have a fractionation effect whose amplitude varies from one element to the other. For instance, a 4°C shift induces a change of 1‰ in δ^{18}O for an equilibrium carbonate [32], but the dependence in temperature of the fractionation of Mg isotopes during carbonate precipitation is less than 0.02‰/amu/°C between 4 and 18°C [33]. In the case of Mg isotopes, a 4°C shift will therefore induce a variation in the δ^{26}Mg lower than 0.16‰. Temperature control on the Zn isotopic composition has so far only been investigated for the precipitation of smithsonite at 30 and 50°C [28]. The fractionation factor is identical at these two temperature [28]. If the results relative to the precipitation of the smithsonite can be applied to the precipitation of carbonate, the range of glacial/interglacial SST variations is unlikely to account for significant Zn fractionation effects, if any.

The variations of both the δ^{18}O record and the δ^{66}Zn record show only slight similarities. Even if glacial/interglacial variations of the Zn isotopic composition cannot be definitively ruled out, the δ^{66}Zn record does not show the glacial/interglacial pattern that is recorded in the eastern equatorial Pacific by paleoproductivity proxies such as carbonate accumulation rates [34], organic carbon accumulation rates [35], benthic foraminifer transfer function [36], and $(^{231}Pa/^{230}Th)_{xs,0}$ in sediments [12]. Although ice volume is an important component of the oxygen isotopic composition of the calcareous shells on the time scale considered in our study, the lack of co-variation between Zn and O isotopic composition in the ODP 849 record is an additional argument against a significant influence of the glacial/interglacial SST variations on the Zn isotope fractionation.

The equatorial Pacific climatic conditions respond strongly to insolation forcing [30,31,37,38]. In order to investigate the possibility of an insolation forcing on the δ^{66}Zn signal, we have calculated a Scargle normalized periodogram [39] of the ODP 849 δ^{66}Zn record. Because of the uneven spacing of the samples on the time

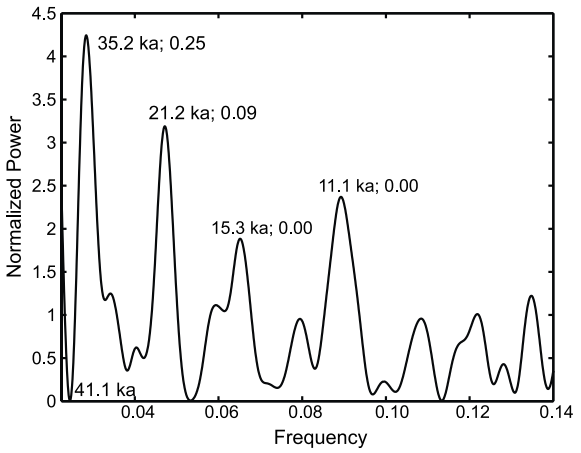

Fig. 5. Scargle normalized periodogram of the δ^{66}Zn residuals after removal of a linear secular trend. The main peaks (frequencies $f=0.028$, 0.047, 0.065 and 0.090) are indicated with the corresponding periods and the values of the F-test (25%, 9%, 0% and 0%, respectively). The 41.1-ka period of the obliquity is also indicated.

scale, the periodogram is a method of choice to investigate the presence of periodic signals.

The signal potentially associated with orbital eccentricity (94.8, 123.8, and 404 ka) [40] is not likely to be observed in the periodogram because the time window covered by the present data is 170 ka. Two techniques have been used with similar results: (1) a linear secular trend was removed from the δ^{66}Zn signal, (2) the signal was smoothed by running a Gaussian filter with different standard deviations (5–10 ka). The residual signal is shown in Fig. 4A. The periodogram of the residuals exhibits two main peaks at 35.2 ka and 21.2 ka (Fig. 5). The false-alarm probability (F-test) performed on these two peaks gives probabilities of 25 and 9%, respectively. Smaller peaks, in particular at 11.1 and 15.3 ka, have no significance (F-test = 0%). Finally, the periodogram exhibits a minimum at the 41.1-ka period characteristic of obliquity, thus showing that the Zn isotopic composition is independent of the obliquity in the eastern equatorial Pacific. This observation is in good agreement (1) with the model of Clement et al. [38] which shows that insolation variations in the tropical Pacific do not exhibit any response to the obliquity cycle, and (2) with observations that insolation in tropical regions responds much more strongly to eccentricity and precession than to obliquity [42,43]. Removal of a parabolic trend or Gaussian filtering neither changes the variance of the residuals nor the period or the relative intensity of the main peaks. Longer periods (e.g. 48.8 ka) are not shown in Fig. 5 since they are likely to result from an artifact (aliasing) due to the small time window covered by the δ^{66}Zn record with regard to this period.

The 35.2-ka period will be discussed later. The theoretical mean period of the precession, 21.7 ka, is very close to the 21.2-ka period observed in our δ^{66}Zn record. The tropical Pacific ocean–atmosphere system responds to precessional forcing [29,37,38]. Seasonal changes in the low-latitude insolation have a strong influence on El Niño/Southern Oscillation-like phenomenon. In particular, precession-induced variations in primary productivity are controlled by changes in the east–west slope of the thermocline [37]. Cold-tongue SST variations in the eastern equatorial Pacific are coherent with precession-induced changes in the seasonality over the last 30 ka [29]. Therefore, in spite of the low significance of the 21.2-ka period in the ODP 849 δ^{66}Zn record, we propose that the δ^{66}Zn signal is modulated by precession.

In tropical regions, the precession cycle controls the intensity of the trade winds [38], which are the prevailing winds in the eastern equatorial Pacific. They converge a few degrees north of the equator. The change in the sign of the Coriolis parameter at the equator induces a south-trade-winds-driven Ekman divergence, the equatorial upwelling (Fig. 1). Nowadays, the south trade winds reach a maximum intensity from August to October [38,43]. As a result, equatorial upwelling intensifies, bringing cold, nutrient-rich water to the surface, thus suppressing the thermocline. By contrast, the intensity of the equatorial upwelling is reduced from February to April in response to weak south trade winds. The resulting development of a steep and deep (100–200 m) thermocline [44] prevents mixing between deep and surface waters.

The strong zonal Zn isotopic variations observed in ferromanganese nodules have been ascribed to the amplitude of seasonal variations in biological productivity [8]. The lighter Zn isotopes in high-latitude surface waters become depleted by biological processes as a result of the development of a seasonal thermocline that prevents the Zn replenishment of the euphotic zone by deep water [8]. Modeling of the tropical Pacific shows that anomalous cooling in the late summer/fall, i.e. reduced insolation during the upwelling season (August–October), slackens the trade winds [38]. Consequently, upwelling is reduced, thus favoring the development of El Niño-like events [38]. The pattern of variations of the ODP 849 δ^{66}Zn record suggests an inverse relation with the equatorial September insolation (Fig. 4A). This feature is less clear during Isotopic Stage 5, which might be due to the lower sampling density. On this basis and on the basis drawn from δ^{66}Zn measurements in Fe–Mn nodules [8], we suggest that the δ^{66}Zn variability in the carbonate fraction of ODP 849 reflects the thermocline steepness in the eastern equatorial Pacific. While lower late-

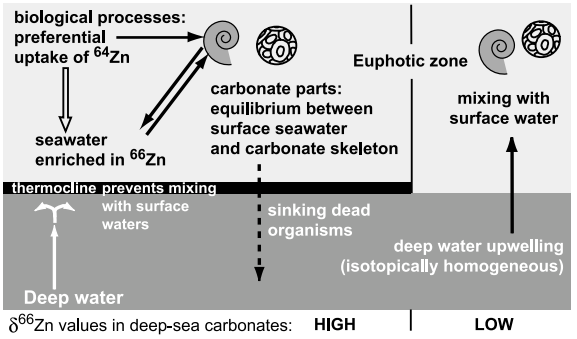

Fig. 6. Scheme of the mechanism proposed to explain the δ^{66}Zn variability in ODP 849. On the left, weak trade winds allow the development of a steep thermocline which prevents the mixing between deep and surface waters. The biological processes preferentially uptake the light Zn isotopes. Therefore the shells grow in water that becomes progressively enriched in ^{66}Zn relative to ^{64}Zn. Since we assume that the carbonate parts of the organisms do not significantly fractionate Zn isotopes, the δ^{66}Zn values of the shells increase progressively until deep water is advected into the surface water (suppression of the thermocline). On the right, strong trade winds and accordingly high upwelling intensity allows the replenishment of surface waters by isotopically homogeneous deep waters.

summer/fall insolation takes place, trade winds weaken during the upwelling season, reducing or suppressing the upwelling, thus allowing the development of a deep and nearly permanent thermocline at the equator. Under such conditions, deep waters do not fully replenish surface waters. Accordingly, surface waters become depleted in the lighter Zn isotopes by biological activity which fractionates Zn isotopes [8]. Consequently, organisms built their shell in a medium which is enriched in the heavier Zn isotopes (Fig. 6). Since we have made the hypothesis of a negligible Zn isotope fractionation between seawater and carbonates, the composition of seawater at the time of organism growth is reflected in the shell of these organisms. When a long-lasting thermocline can develop, the shell exhibits high δ^{66}Zn values that are therefore recorded in sediments after the death of the organisms. On the contrary, low δ^{66}Zn values in carbonate sediments correspond to periods of strong trade winds during the upwelling season. High-intensity trade winds prevent the development of a thermocline. This hypothesis is supported by the agreement between the pattern of variation of the δ^{66}Zn record and the 500-yr average NINO3 index forced by insolation [38] (Fig. 4B): positive SST anomalies in the equatorial eastern Pacific corresponding to higher δ^{66}Zn, which, according to our hypothesis, corresponds to times when a steep and deep thermocline develops. The SST pattern of core VNTR01-8PC (the site-survey piston core of ODP 849) [45] reconstructed from a radiolarian transfer function is similar to the δ^{66}Zn record with less high-frequency variability. There is a good correspondence between some high SST and high δ^{66}Zn peaks (20–25 ka, 30 ka, 78 ka) and vice versa (34 ka, 49 ka, 142 ka). Higher average δ^{66}Zn values during Isotopic Stage 5 seem to correspond to higher average SST. Better correlation is hard to define because of the lack of resolution of the two age models used in the two cores.

A ca. 31-ka period has been noticed in sedimentary records from the tropical Indian and Pacific oceans ([37] and references therein) and was seen as a non-linear response of tropical origin and interpreted to reflect changes in local wind intensity [45]. We have found a similar 35-ka period in the ODP 849 δ^{66}Zn record. This supports the hypothesis of a variability of the Zn isotopic composition modulated by the intensity of the trade winds.

6. Conclusion

Our measurements show a good reproducibility (usually <0.07‰). The results presented in this study show high-amplitude (1‰) variations in the Zn isotopic composition of the carbonate fraction of ODP core 849. In the eastern equatorial Pacific these variations appear to have two periods of 21.2 and 35.2 ka. The 21.2-ka period is close to the average period of the precession; therefore we have made the hypothesis that the δ^{66}Zn record of ODP 849 is modulated by the precession cycle. The idea that Zn isotopic compositions in the carbonate fraction of deep-sea sediments are reflecting climate changes is supported by our observations. The ODP 849 δ^{66}Zn pattern appears to have an inverse relationship

with the equatorial late-summer/fall insolation which controls the strength of the equatorial upwelling through the intensity of the trade winds. The variations in the Zn isotopic composition have therefore been related to the steepness of the thermocline controlled by the intensity of the trade winds. The temporary isolation of the ocean euphotic layer where most of the biological activity (which preferentially seems to remove the lighter Zn isotopes) takes place is suggested to be induced by the precession and unrelated to the obliquity, while the time interval covered by the core investigated does not allow us to assess the role of eccentricity.

Acknowledgements

Philippe Télouk is deeply thanked for keeping the Plasma 54 in top running condition. We also thank Albert Galy, Thomas M. Marchitto and Ariel D. Anbar for their detailed and constructive reviews. This study was supported financially by the French Ministère de l'Education Nationale, de la Recherche et de la Technologie and the French Institut National des Sciences de l'Univers. *[BARD]*

References

[1] T. Takahashi, R.A. Feely, R.F. Weiss, R.H. Wanninkhof, D.W. Chipman, S.C. Sutherland, T.T. Takahashi, Global air-sea flux of CO_2: an estimate based on measurements of sea-air pCO_2 difference, Proc. Natl. Acad. Sci. USA 94 (1997) 8292–8299.

[2] J.H. Martin, S.E. Fitzwater, Iron deficiency limits phytoplankton growth in the north-east Pacific subarctic, Nature 331 (1988) 341–343.

[3] F.M.M. Morel, J.R. Reinfelder, C.P. Chamberlain, S.B. Roberts, J.G. Lee, D. Yee, Zinc and carbon co-limitation of marine phytoplankton, Nature 369 (1994) 740–742.

[4] K.W. Bruland, G.A. Knauer, J.H. Martin, Zinc in northeastern Pacific waters, Nature 271 (1978) 741–743.

[5] J.J.R. Fraústo da Silva, R.J.P. Williams, The Biological Chemistry of Elements: The Inorganic Chemistry of Life, Clarendon Press, Oxford, 1991, 206 pp.

[6] S.J. Lippard, J.M. Berg, Principles of Bioinorganic Chemistry, University Science Books, Mill Valley, 1994, 411 pp.

[7] N.A. Nimer, L.F. Dong, Q. Guan, M.J. Merrett, Calcification rate, dissolved inorganic carbon utilization and carbonic anhydrase activity in *Emiliania huxleyi*, Bull. Inst. Oceanogr. Monaco 14 (1995) 43–49.

[8] C.N. Maréchal, E. Nicolas, C. Douchet, F. Albarède, The abundance of zinc isotopes as a marine biogeochemical tracer, Geochem. Geophys. Geosyst. 1 (2000) 1999GC-000029.

[9] F.P. Chavez, K.R. Buck, R.T. Barber, Phytoplankton taxa in relation to primary production in the equatorial Pacific, Deep-Sea Res. 37 (1990) 1733–1752.

[10] C.N. Maréchal, P. Telouk, F. Albarède, Precise analysis of copper and zinc isotopic compositions by plasma-source mass spectrometry, Chem. Geol. 156 (1999) 251–273.

[11] Shipboard Scientific Party, Site 849, in: L. Mayer et al. (Eds.), Proc. ODP Init. Rep. 138 (part 2), (1992) 735–807.

[12] S. Pichat, K.W.W. Sims, R. François, J.F. McManus, F. Albarède, Lower biological productivity during glacial periods in the equatorial Pacific as derived from $(^{231}Pa/^{230}Th)_{xs,0}$ measurements in deep-sea sediments (in preparation).

[13] J.R. Toggweiler, K. Dixon, W.S. Broecker, The Peru upwelling and the ventilation of the South Pacific thermocline, J. Geophys. Res. 96 (1991) 20467–20497.

[14] A.C. Mix, N.G. Pisias, W. Rugh, J. Wilson, A. Morey, T.K. Hagelberg, Benthic foraminifer stable isotope record from site 849 (0-5 Ma): local and global climate changes, in: N.G. Pisias et al. (Eds.), Proc. ODP Sci. Results 138 (1995) 371–412.

[15] T.K. Hagelberg, N.G. Pisias, N.J. Shakleton, A.C. Mix, S. Harris, Refinement of a high-resolution continuous sedimentary section for the study of the equatorial Pacific paleoceanography ODP Leg 138, in: N.G. Pisias et al. (Eds.), Proc. ODP Sci. Results 138 (1995) 47–57.

[16] T.B. Coplen, J.K. Böhlke, P. De Bièvre, T. Ding, N.E. Holden, J.A. Hopple, Isotope-abundance variations of selected elements (IUPAC technical report), Pure Appl. Chem. 74 (2002) 1987–2017.

[17] T.M. Marchitto, W.B. Curry, D.W. Oppo, Zinc concentrations in benthic foraminifera reflect seawater chemistry, Paleoceanography 15 (2000) 299–306.

[18] E.A. Boyle, Cadmium, zinc, copper, and barium in foraminifera tests, Geochim. Cosmochim. Acta 47 (1983) 1815–1819.

[19] E.A. Boyle, L.D. Keigwin, Comparison of Atlantic and Pacific paleochemical records for the last 215,000 years: Changes in deep ocean circulation and chemical inventories, Earth Planet. Sci. Lett. 76 (1985/86) 135–150.

[20] S. Ray, H.R. Gault, C.G. Dodd, The separation of clay minerals from carbonate rocks, Am. Mineral. 42 (1957) 681–686.

[21] R. Chester, M.J. Hughes, A chemical technique for the separation of ferromanganese minerals, carbonate minerals, and adsorbed trace elements from pelagic sediments, Chem. Geol. 2 (1967) 249–262.

[22] A. Koschinsky, P. Halbach, sequential leaching of marine ferromanganese precipitates: Genetic implications, Geochim. Cosmochim. Acta 59 (1995) 5113–5132.

[23] Y.W. Heo, H.B. Lim, Determination of inorganic species in the solution extracted from cleanroom gloves used in semiconductor process, Bull. Korean Chem. Soc. 20 (1999) 226–228.
[24] A.D. Anbar, K.A. Knap, J. Barling, Precise determination of mass-dependent variations in the isotopic composition of Molybdenum using MC-ICPMS, Anal. Chem. (2001) 1425–1431.
[25] J. Imbrie, J.D. Hays, D.G. Martinson, A. McIntyre, A.C. Mix, J.J. Morley, N.G. Pisias, W.L. Prell, N.J. Shackleton, The orbital theory of Pleistocene climate: Support from a revised chronology of the marine $\delta^{18}O$ record, in: A. Berger et al. (Eds.), Milankovitch and Climate, Part 1, Series C: Mathematical and Physical Sciences 126, D. Reidel, Dordrecht, 1984, pp. 269–305.
[26] S.V. Margolis, P.M. Kroopnick, D.E. Goodney, W.C. Dudley, M.E. Mahoney, Oxygen and carbon isotopes from calcareous nannofossils as paleoceanographic indicators, Science 189 (1975) 555–557.
[27] F.J. Millero, Chemical Oceanography, CRC Press, Boca Raton, FL, 1996, 496 pp.
[28] C.N. Maréchal, S.M.F. Sheppard, Isotopic fractionation of Cu and Zn between chloride and nitrate solutions and malachite or smithsonite at 30° and 50°C, Geochim. Cosmochim. Acta 66 (2002) S484.
[29] C.N. Maréchal, F. Albarède, Ion-exchange fractionation of copper and zinc isotopes, Geochim. Cosmochim. Acta 66 (2002) 1499–1509.
[30] M.A. Cane, A role for the tropical Pacific, Science 282 (1998) 59–61.
[31] A. Koutavas, J. Lynch-Stieglitz, T.M. Marchitto, J.P. Sachs, El Nino-like pattern in ice age tropical Pacific sea surface temperature, Science 297 (2002) 226–230.
[32] S.-T. Kim, J.R. O'Neil, Equilibrium and nonequilibrium oxygen isotope effects in synthetic carbonates, Geochim. Cosmochim. Acta 61 (1997) 3461–3475.
[33] A. Galy, M. Bar-Matthews, L. Halicz, R.K. O'Nions, Mg isotopic composition of carbonate: insight from speleothem formation, Earth Planet. Sci. Lett. 201 (2002) 105–115.
[34] D.E. Archer, Equatorial Pacific calcite preservation cycles: production or dissolution?, Paleoceanography 6 (1991) 561–571.
[35] M. Lyle, D.W. Murray, B.P. Finney, J. Dymond, J.M. Robbins, K. Brooksforce, The record of the late Pleistocene biogenic sedimentation of the eastern tropical Pacific Ocean, Paleoceanography 3 (1988) 39–59.
[36] P. Loubere, Marine control of biological production in the eastern equatorial Pacific Ocean, Nature 406 (2000) 497–500.
[37] L. Beaufort, T. de Garidel-Thoron, A.C. Mix, N.G. Pisias, ENSO-like forcing on oceanic primary production during the late Pleistocene, Science 293 (2001) 2440–2444.
[38] A.C. Clement, R. Seager, M.A. Cane, Orbital controls on the El Niño/Southern Oscillation and the tropical climate, Paleoceanography 14 (1999) 441–456.
[39] J.D. Scargle, Studies in astronomical time series II: Statistical aspects of spectral analysis of unevenly spaced data, Astrophys. J. 263 (1982) 835–853.
[40] A.L. Berger, M.F. Loutre, Insolation values for the climate of the last 10 million years, Quat. Sci. Rev. 10 (1991) 297–317.
[41] A. Berger, Numerical values of mid-month insolation from 1,000,000 YBP to 100,000 YAP (astronomical solution of Berger, 1978), in: Contribution No. 36, Université Catholique de Louvain, Institut d'Astronomie et de Géophysique G. Lemaitre, Louvain-la-Neuve, 1978.
[42] A. McIntyre, B. Molfino, Forcing of Atlantic equatorial and subpolar millennial cycles by precession, Science 274 (1996) 1867–1870.
[43] P.E. Hays, N.G. Pisias, A.K. Roelofs, Paleoceanography of the eastern equatorial Pacific during the Pliocene: A high resolution study, Paleoceanography 4 (1989) 57–73.
[44] L.D. Talley, G. Fryer, R. Lumpkin, Physical oceanography of the tropical Pacific, in: M. Rapaport (Ed.), Geography of the Pacific Islands, Bess Press, Honolulu, HI, 1998, pp. 19–32.
[45] N.G. Pisias, A.C. Mix, Spatial and temporal oceanographic variability of the eastern equatorial Pacific during the late Pleistocene: evidence from radiolaria microfossils, Paleoceanography 12 (1997) 381–393.